MARS ADVANCED RADAR FOR SUBSURFACE AND IONOSPHERE SOUNDING (MARSIS): SUBSURFACE PERFORMANCES EVALUATION

G.Picardi, University "La Sapienza" – INFOCOM Dpt., Rome, Italy. picar@infocom.uniroma1.it
D.Biccari, A.Bazzoni, F.Fois, M.Iorio, R.Seu, University "La Sapienza" – INFOCOM Dpt., Rome, Italy.
P.Melacci, University of Perugia – Dept. of Physics – Perugia, Italy
C.Federico, A.Frigeri, G.Minelli, University of Perugia – Dept. of Geology – Perugia, Italy
L.Marinangeli, IRSPS, University G.D'Annunzio, v. Pindaro 42, Pescara, Italy
R. Orosei, CNR/IAS - Planetology Dept. – Rome - Italy
D.Calabrese, E.Zampolini, Remote Sensing Engineering, Alenia Spazio, Rome, Italy.
W.T.K.Johnson, R.L.Jordan, J.Plaut, A.Safaenili, JPL – Pasadena-USA

Keywords: MEX mission, MARSIS, Radar Sounding, Planetary missions

Abstract

According to the Mars Express mission, the MARSIS primary *scientific objectives* are to *map the distribution of water, both liquid and solid, in the upper portions of the crust of Mars*. Three *secondary objectives* are also defined *subsurface geologic probing, surface characterization,* and *ionosphere sounding*.

In order to obtain the primary objectives the Radar Sounder design was based on the *Ice/water interface* and *Dry/ice interface* scenario: defining the material composition of the first layers and porosity and the pore filling materials. Concerning the surface, we have characterized the geometric structure in terms of a *large-scale* morphology, on which a *small-scale* geometric structure, due to rocks, is superimposed, taking into account also that recently the structure of the planets surface was described by means of fractals and in particular the new MARS surface models obtained by processing of the MOLA data.

According to these models, this paper provides a description of the operational planning approach and expected performances of MARSIS.

1 INTRODUCTION

MARSIS is a low-frequency nadir-looking pulse limited radar sounder and altimeter with ground penetration capabilities, this radar can effectively operate at any altitude lower than 800 km. In order to maximize the penetration capabilities of the transmitted pulse MARSIS must operate at a frequency as low as possible as carrier frequencies taking into account the expected values of the plasma frequency in the Martian ionosphere: 1.8, 3, 4 and 5 MHz was selected. Moreover the requirement of fine range resolution entails a relatively large transmitted bandwidth (1 MHz), so that MARSIS will operate with a very high fractional bandwidth: a 1 MHz bandwidth allows a vertical resolution of 150 m in vacuum which corresponds to 50-100 m in the subsurface, depending on the e.m. wave propagation speed in the crust.

According to the well known principle of operation of a subsurface radar, a short pulse of e.m. energy transmitted by the antenna impinging on the top of the Mars surface produce a first reflection echo, which propagates backward to the radar, moreover, thanks to the long wavelengths employed, a significant fraction of the e.m. energy impinging on the surface is transmitted into the crust and propagates downward. Additional reflections, due to the subsurface dielectric discontinuities would occur and the relevant echoes would propagate backward through the first layer medium and then to the radar generating further echo signals, much weaker than the front surface signal. The time delay of the echo can be converted to a depth, assuming that the propagation speed of the medium is known, and the intensity of the reflection can be analyzed to estimate the reflectivity at the interface and the attenuation properties of the intervening layers.

In order to optimize the radar design, according to the suggestions from planetary scientists, we have selected some models of subsurface porosity profile and composition, as described in the following. Moreover the two most likely scenarios representing the relevant interfaces are the following:

Ice/water(I/W) interface – in this scenario the pores are filled with ice from the surface down to a depth below which liquid water is stable and becomes the pore-filling material. The change of the pore-filling material causes a discontinuity of the overall dielectric constant, which can be detected by the radar sounder.

Dry/ice(D/I) interface - here the pore-filling material is considered to be gas or some other vacuum-equivalent material up to a depth, below which ice fills the pores. Hence the interface to detect is between dry regolith and ice-filled regolith.

We can notice that a dynamic range of 50-60 dB can be managed by the instrument, but there are several factors that can strongly reduce the detection dynamic mainly the noise and the surface clutter In fact due to the orbital sounding geometry, the off nadir surface return will be received at the same time of subsurface echoes. Then, in case of rough surface, the surface echoes may happen to hide weak subsurface features and the detection of discontinuities in the crust could be indered by surface clutter. As more the surface is smooth as more rapidly the returns from the surface at off-nadir angles will drop off.

Hence it is important to evaluate the penetration depth that is possible to reach according to the transmitted wavelength the dielectric characteristics of the crust and the surface scattering behavior as a function of the surface topography. which uses synthetic aperture techniques and a secondary receiving antenna to isolate subsurface reflections.

Moreover different techniques are envisaged to increase the detection performance against surface clutter. First of all the *Doppler Azimuth Processing* significantly reduces the surface echoes coming from along track off nadir reflections: the improvement on the overall surface clutter attenuation should be of the order of 10 dB.

Report Documentation Page

Form Approved
OMB No. 0704-0188

1. REPORT DATE	2. REPORT TYPE	3. DATES COVERED
14 APR 2005	**N/A**	**-**

4. TITLE AND SUBTITLE	5a. CONTRACT NUMBER
Mars Advanced Radar For Subsurface And Ionosphere Sounding (Marsis): Subsurface Performances Evaluation	5b. GRANT NUMBER
	5c. PROGRAM ELEMENT NUMBER
6. AUTHOR(S)	5d. PROJECT NUMBER
	5e. TASK NUMBER
	5f. WORK UNIT NUMBER
7. PERFORMING ORGANIZATION NAME(S) AND ADDRESS(ES) **University La Sapienza INFOCOM Dpt., Rome, Italy.**	8. PERFORMING ORGANIZATION REPORT NUMBER
9. SPONSORING/MONITORING AGENCY NAME(S) AND ADDRESS(ES)	10. SPONSOR/MONITOR'S ACRONYM(S)
	11. SPONSOR/MONITOR'S REPORT NUMBER(S)

12. DISTRIBUTION/AVAILABILITY STATEMENT
Approved for public release, distribution unlimited

13. SUPPLEMENTARY NOTES
See also ADM001798, Proceedings of the International Conference on Radar (RADAR 2003) Held in Adelaide, Australia on 3-5 September 2003., The original document contains color images.

14. ABSTRACT

15. SUBJECT TERMS

16. SECURITY CLASSIFICATION OF:			17. LIMITATION OF ABSTRACT	18. NUMBER OF PAGES	19a. NAME OF RESPONSIBLE PERSON
a. REPORT	b. ABSTRACT	c. THIS PAGE			
unclassified	**unclassified**	**unclassified**	**UU**	**7**	

Then the instrument *secondary antenna, a monopole* oriented along the nadir axis, will receive mostly the off-nadir surface returns, that could be thus subtracted by the primary antenna composite signal, further reducing the surface clutter level (about ~15dB).
Finally echo profiles collected at *two different frequencies* can be processed to separate the subsurface reflections, which are strongly dependent on the frequency, from the surface reflections, which are mostly frequency independent (the achieved improvement can reach 10-15 dB) and to have information of the first layer attenuation.

2 SURFACE AND SUBSURFACE SCATTERING MODELS

In order to estimate the reflectivity at the interface and the attenuation properties of the intervening layers and to assess the interface detection performance it is required to evaluate the back scattering cross sections of concurrent echoes coming from the surface and subsurface layers:
$\sigma_s = \Gamma_s \cdot f_s(H_s, s_s, \lambda)$ $\sigma_{ss} = \Gamma_{ss} \cdot f_{ss}(H_{ss}, s_{ss}, \lambda)$
being Γ_S and Γ_{SS} the Fresnel reflectivity terms, which deal with the surface and subsurface dielectric properties and f_s and f_{ss} the scattering terms, which deal with the geometric structure of the surface and subsurface.

2.1 Fresnel coefficients and subsurface attenuation

In Tab.1 are listed the values of dielectric constant of the materials which can be considered as end members of the range in which the first layer of the Martian surface materials may vary. The dielectric properties of the water and ice filling the pores are listed in the Tab.2.
It should be noted that, since porosity depends on the depth, so will do the effective dielectric constants of the mixture. In order to evaluate the mixture dielectric constants, we have used the Maxwell-Garnett model

(2.1.1) $$\varepsilon_m(z) = \varepsilon_h \frac{1 + 2\phi(z)y}{1 - \phi(z)y}$$

where $y = \frac{\varepsilon_i - \varepsilon_h}{\varepsilon_i + 2\varepsilon_h}$ and the porosity at depth z is

(2.1.2) $$\Phi(z) = \Phi(0) e^{-\frac{z}{K}}$$

	ε_{rh}	Tangδ
I	5	0.004
II	9	0.03
III	7.1	0.014

Tab.1

	ε_{ri}	tangδ
Gas	1	0
Ice	3.15	0.0002
Water	88	0.0001

Tab.2

In (2.1.2) K is the decay constant that, for Mars, can be computed by scaling the measured Lunar decay constant for the ratio between the Lunar and Martian surface gravitational accelerations, under the assumption of comparable crust densities: the resulting value for Mars is K=2.8 km.
Using the eq.(2.1.1), the effective dielectric constant of the mixtures which have been selected to represent the Martian porous regolith can be evaluated, as a function of the depth, and of the surface porosity. Therefore the well known *Surface Fresnel reflectivity* for nadir incidence (from free space propagation) can be evaluated

(2.1.3) $$\Gamma^S = \left| \frac{\sqrt{\varepsilon_{r1}(0)} - 1}{\sqrt{\varepsilon_{r1}(0)} + 1} \right|^2 = R_{01}^2$$

being $\varepsilon_{r1}(0)$ the real dielectric constant of the crust evaluated at the surface (z=0).

The selected models make the surface reflectivity ranging between -6.5 dB and -9.5 dB for the I/W scenario and -7 dB and -12 dB for the D/I scenario.

	$\Gamma_{s\,\mid dB}$			
	I/W		D/I	
	50%	20%	50%	20%
I	-9.5	-9	-12	-9.5
II	-7.5	-6.5	-9	-7
III	-8.5	-7.5	-10	-8

Tab.3

The Fresnel reflectivity for a subsurface layer located at a depth z' can be expressed as follows

(2.1.4) $$\Gamma_{SS,z'} = R_{12,z'}^2 \left(1 - R_{01}^2\right)^2 10^{-0.1\int_0^{z'} \alpha(z)dz}$$

being $R^2_{12,z'}$ the reflection coefficient of such interface:

(2.1.5) $$R^2_{12,z'} = \left| \frac{\sqrt{\varepsilon_{r1}(z')} - \sqrt{\varepsilon_{r2}(z')}}{\sqrt{\varepsilon_{r1}(z')} + \sqrt{\varepsilon_{r2}(z')}} \right|^2$$

By the defined crust materials, we have obtained for the two scenario:

(2.1.6)
$$\text{I/W} \rightarrow R^2_{12,z'} \cong (-10 \div -18) - 3\text{dB/Km}$$
$$\text{D/I} \rightarrow R^2_{12,z'} \cong (-20 \div -28) - 3\text{dB/Km}$$

where the first term is related to the first layer porosity and the last one is due to the decreasing of the porosity with the depth. We can notice that the $R^2_{12,z'}$ is near crust material independent.
Concerning the two way attenuation:

(2.1.7) $$\alpha_{dB/m}(z) = 1.8 \cdot 10^{-7} f_0 \sqrt{\varepsilon(z)} \tan\delta(z)$$

we have obtained, as a good approximation, the functions detailed in Tab.4.

	$\alpha(z)\,\mid$ dB/KmMHz			
	I/W		D/I	
	50%	20%	50%	20%
I	(0.8+0.1z)	(1.3+0.05z)	(0.9+0.1z)	(1.3+0.05z)
II-1/III	(3.7+0.54*z)	(6+0.25*z)	(4.3+0.54*z)	(6.3+0.25*z)
II-2	(8.5+1.1*z)	(13.3+0.5*z)	(9.5+1.1*z)	(13.7+0.5*z)

Tab.4 (z depth in Km)

2.2 Surface backscattering models

At the beginning of our analysis we modeled the Martian surface back scattering considering two main terms: the first, called *large scale scattering contribution*, resulting from gentle geometrical undulations of the surface on a scale of many hundreds to thousands meters, whereas the second, called *small scale scattering contribution*, giving reason of the fast, slight variations of the surface height over an horizontal scale of some tenths of meters. A plausible range for the parameters describing the surface geometry is listed in the Tab.5.

LARGE SCALE MODEL		**SMALL SCALE MODEL**	
RMS slope (m_s)	Correlation Length	RMS Slope	RMS height
0.01 - 0.1 rad. (0.57°-5.7°)	*200 – 30000 m*	*0.1 – 0.6 rad. (5.7° - 34.3°)*	*0.1 – 1 m*

Tab.5: *Summary of the values range for the geometric parameters of the surface*

From the statistical point of view, the surface height was be modeled as a Gaussian random process, being σ_h the total surface RMS height. At a second order level we suppose (as usual) an isotropic correlation coefficient.
Simple approximate methods can be applied for surfaces which present a unique roughness scale, with either a big correlation length (gently undulating surface), or a very small rms height (slightly rough surface) compared to the incident wavelength. Specifically, the Kirchhoff method can be applied for gently undulating surfaces, which respect the tangent plane conditions and the Small Perturbation Method can be applied to slightly rough surfaces. The classical studies on the validity conditions of these two models [1] have been recently updated [2], and regions of validity currently defined are reported in Fig.1. It is evident from these figures that the Kirchhoff approximation can be used to evaluate the large scale backscattering contribution whereas the Small perturbation method can be used for the small scale contribution.

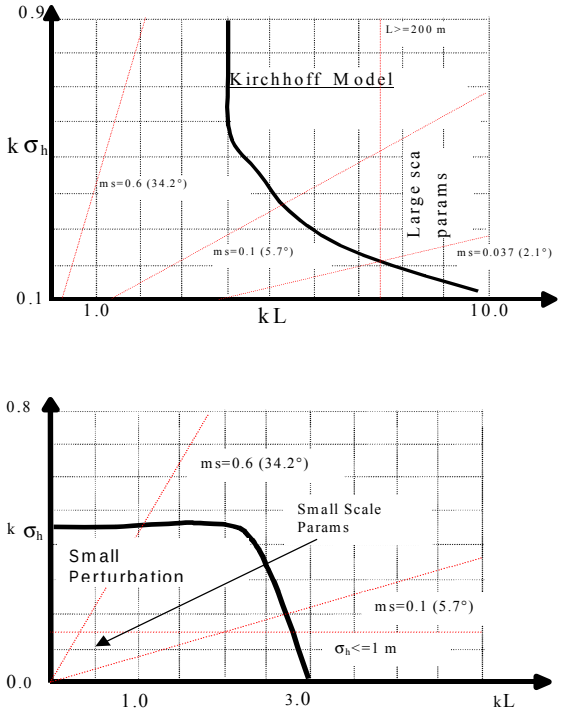

Fig.1: KIRCHHOFF and SMALL PERTURBATION approximation validity conditions (k=2π/λ)

2.2.1 *Large Scale Contribution evaluation*

Under Kirchhoff approximation hypotheses the scattered electric field to the antenna is given by the following integral [1]:

$$(2.2.1)\quad E_S(t)=\frac{1}{2\pi}\int_{-\infty}^{\infty}F(\omega)\cdot\left(-\frac{j}{2\lambda}\right)\int_S G(P)\cdot R(P)\cdot\frac{\hat{n}\cdot\left(2\hat{R}_1\right)}{R_1^2}\cdot e^{-jk2R_1}dS\cdot e^{j\omega}d\omega$$

where $E_i=(1/R_1)e^{-jkR}{}_1$ is the incident spherical wave, F(ω) is the Fourier transform of the transmitted pulsed waveform, λ is the wavelength, P is the generic point on the surface, *G(P)* is the antenna normalized gain in the direction of the point *P* on the surface *S*, *R(P)* is the Fresnel coefficient, R_1 is the distance from radar to the point *P*, $\hat{R}_1$ is the unit vector corresponding to the path from the radar to the point *P*, $\hat{n}$ is the unit vector normal to the surface in the point *P* and finally $k=2\pi/\lambda$ is the wave number.
If we make the further hypotheses of Isotropic antenna pattern and surface tilts are small enough to allow that we confuse the local normal to the surface with the vertical axis, we have G(P)=1 and $\hat{n}\cdot\hat{R}_1\approx\hat{z}\cdot\hat{R}_1=\cos\theta$, where θ is the incidence angle with respect to the vertical. Moreover the distance from the radar to the generic point P(x,y,z) can be approximated, under the far-field approximation, as:

$$(2.2.2)\quad R_1\approx h-z\cos\theta+\frac{x^2+y^2}{2h}$$

where h is the distance from the Radar to the mean surface. With all these assumptions the eq. (2.2.1) becomes:

$$(2.2.3)\quad E_S(\tau)=-\frac{2\cos\theta}{4\pi\cdot ch}R(\theta)\int_S dS\int_{-\infty}^{\infty}e^{j\omega\left(\tau-\frac{x^2+y^2}{h\cdot c}+\frac{2z\cdot\cos\theta}{c}\right)}j\omega F(\omega)d\omega$$

where $\tau=t-\frac{2h}{c}$ and the angle of incidence has been supposed to undergo no significant variation within the pulse limited integration area, and has been therefore taken out of the surface integral.
The average scattered power at time τ can be evaluated taking the average of the product of the scattered electric field with its complex conjugate:

$$\left\langle E_S(\tau)\cdot E_S^*(\tau)\right\rangle=\frac{4\Gamma_s(\theta)}{\left(4\pi\cdot ch^2\right)^2}\cos^2\theta\int d\omega_1\int d\omega_2\omega_1\cdot\omega_2F(\omega_1)F^*(\omega_2)e^{j(\omega_1-\omega_2)\tau}\cdot$$

$$(2.2.4)\quad \cdot\int_{S_1}dS_1\int_{S_2}dS_2\cdot e^{-\frac{j}{ch}\left[\omega_1\left(x_1^2+y_1^2\right)-\omega_2\left(x_2^2+y_2^2\right)\right]}\cdot\left\langle e^{j\frac{2\cos\theta}{c}(\omega_1z_1-\omega_2z_2)}\right\rangle$$

where $\Gamma_s(\theta)=\left|R(\theta)\right|^2$ is the Fresnel reflection coefficient. The average on the height z can be expressed as a function of the surface two-dimensional characteristic function:

$$(2.2.5)\quad \left\langle e^{j\frac{2\cos\theta}{c}(\omega_1z_1-\omega_2z_2)}\right\rangle=e^{-2\sigma_{h1}^2\frac{\cos^2\theta}{c^2}\left(\omega_1^2+\omega_2^2-2\rho(x_1,x_2,y_1,y_2)\omega_1\omega_2\right)}$$

The solution of the integral is not easily achievable in the general case: a closed form has been derived [4] assuming a gaussian correlation coefficient (gaussian roughness spectrum):

$$(2.2.6)\quad \rho(\xi)=e^{-\frac{\xi^2}{L^2}}\quad\Leftrightarrow\quad S(j\omega)=\frac{\sigma_P}{\sqrt{\pi}}e^{-\sigma_P{}^2\omega^2}$$

$$\rightarrow\ F(\omega)=\frac{1}{2}\left\{S\left[j(\omega-\omega_o)\right]+S\left[j(\omega+\omega_o)\right]\right\}$$

which corresponds to a gaussian shape for the compressed pulse

$$(2.2.7)\quad f(t)=e^{-\frac{t^2}{4\sigma_P^2}}\cos\omega_0t$$

where ω_o is the carrier frequency and σ_P is related to the system bandwidth B_W: $\sigma_P\approx\frac{0.37}{B_W}$.
These hypotheses lead to the following results [4]:

$$(2.2.8)\quad \left\langle E_S(\tau)E_S^*(\tau)\right\rangle=\Gamma_s(\theta)\frac{1}{4h^2}\cos^2\theta\left(P_c+P_{nc1}-P_{nc2}\right)$$

where P_c (τ) is the *coherent (specular)* scattering component:

$$(2.2.9)\quad P_c(\tau)=\frac{1}{1+F}e^{-\frac{(2k\sigma_{h1}\cos\theta)^2}{1+F}}\cdot e^{-\frac{\tau^2}{2\sigma_P^2(1+F)}}$$

while $P_{nc}(\tau)=P_{nc1}(\tau)-P_{nc2}(\tau)$ is the *non-coherent (diffuse)* scattering component:

$$P_{nc1}(\tau)=\frac{\beta}{\sqrt{1+2F}}\sqrt{\frac{\pi}{2}}\cdot e^{\frac{\beta^2}{2}}\cdot e^{-\beta\frac{\tau}{\sigma_p\sqrt{1+2F}}}\cdot Erfc\left[\frac{1}{\sqrt{2}}\left(\beta-\frac{\tau}{\sigma_p\sqrt{1+2F}}\right)\right]$$

(2.2.10)
$$P_{nc2}(\tau)=\frac{\beta}{\sqrt{1+F}\cdot\sqrt{1+2F}}\sqrt{\frac{\pi}{2}}\cdot e^{\frac{(2k\sigma_{h1}\cos\theta)^2}{1+F}}\cdot e^{\frac{\beta^2(1+F)}{2(1+2F)}}\cdot e^{-\beta\frac{\tau}{\sigma_p\sqrt{1+2F}}}$$
$$\cdot Erfc\left[\frac{1}{\sqrt{2}}\left(\beta\sqrt{\frac{1+F}{1+2F}}-\frac{\tau}{\sigma_p\sqrt{1+F}}\right)\right]$$

where:

(2.2.11)
$$F=\frac{1}{2}\frac{\sigma_{h1}^2\cos^2\theta}{\left(\frac{c\sigma_P}{2}\right)^2}\qquad \textit{normalized roughness}$$

(2.2.12)
$$\sigma_{eq}=\sqrt{\sigma_P^2+\left(\frac{2\sigma_{h1}\cos\theta}{c}\right)^2}=\qquad \textit{equivalent pulse width}$$
$$=\sigma_P\sqrt{1+2F}$$

(2.2.13)
$$\beta=\frac{c\sigma_P}{2h}\frac{\sqrt{1+2F}}{m_s^2\cos\theta}\left(1-e^{-(2k\sigma_{h1}\cos\theta)^2}\right)$$

surface parameter

Therefore the cross section of the large scale surface model is given by:

(2.2.14)
$$\sigma_1(\tau)=\frac{\langle E_S(\tau)E_S^*(\tau)\rangle}{\langle E_I(\tau)E_I^*(\tau)\rangle}4\pi h^2=\Gamma_s(\theta)\pi h^2\cos^2\theta\ \left(P_c+P_{nc1}-P_{nc2}\right)$$

We can notice that the maximum power is received when full coherent reflection occurs, i.e. when the surface is perfectly flat ($\sigma_{h1}=0$). In such a condition it is easy to verify that $P_{nc1}=P_{nc2}$ and the non-coherent term P_{nc} reduces to zero, while the coherent term P_c approaches the shape of the transmitted pulse, which is maximum for $\tau = 0$ so that:

(2.2.15)
$$\sigma_{1,MAX}(0)=\Gamma_s(0)\pi h^2$$

which is a value consistent with well know result for perfectly flat surfaces reflection coefficient. As the surface becomes rougher (σ_{h1} increases, $\sigma_{h1} >> \lambda$) the coherent component goes towards zero and non-coherent scattering becomes dominant (geometrical optics model):

(2.2-16)
$$\sigma_{1MAX,NC}(\tau)\approx\Gamma_s(0)\pi h^2\frac{\beta}{\sqrt{1+2F}}\sqrt{\frac{\pi}{2}}\cdot 2\cdot e^{-\frac{\beta^2}{2}}\approx$$
$$\approx\Gamma_s(0)\pi h\frac{c\sigma_P}{2}\sqrt{2\pi}\frac{1}{m_s^2}\approx\Gamma_s(0)\pi h\frac{c}{2\cdot B_w}\frac{1}{m_s^2}$$

being $\sqrt{2h\frac{c}{2\cdot B_w}}$ the radius of pulse-limited region of conventional altimeter mode.

In the following our attention will be devoted only to the maximum of the return waveform.

2.2.2 Fractal Surface topography model

Following, recent attempts to describe the structure of the planets surface by means of fractals, and several papers on the analysis of MOLA (Mars Orbital Laser Altimeter) data, from the Mars Global Surveyor, we tried to introduce this model in our instrument performance evaluation. We wish to recall that MOLA is Laser altimeter whose data can be reduced to topographic height and, due to the time interval between the measurement, are spaced of about 300 m. In particular it was outlined (s. e.g. Fig.2a) from [7]) that Mars surface point to point slope seems to display a power law behavior vs. the lag distance typical in fractal profile and the parameter that drives the scaling behavior is called Hurst exponent H. Moreover by considering larger values of lag distance we have obtained a best fitting, by experimental analysis, with the classical stationary Gaussian amplitude model correlated with exponential correlation function

(2.2-17)
$$\rho(\Delta x)=\exp\left(-\frac{|\Delta x|^{2H}}{L_f^{2H}}\right)$$

We wish remember the approximation with the well known

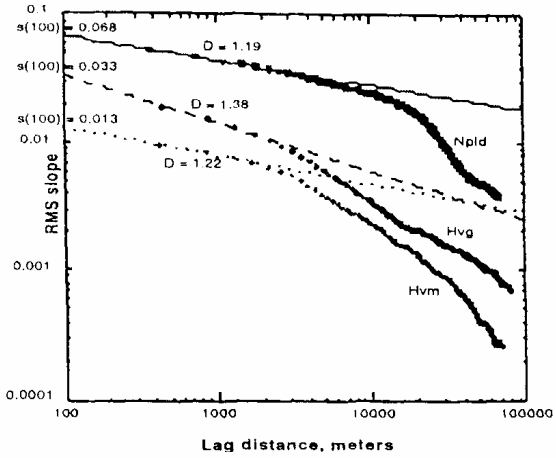

a)

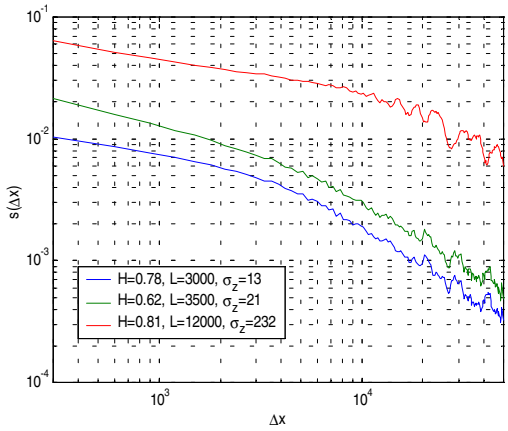

Fig.2b)

Fractal correlation function [5]:

(2.2-18)
$$\rho(\Delta x)=\exp\left(-\frac{|\Delta x|^{2H}}{L_f^{2H}}\right)\approx 1-\frac{|\Delta x|^{2H}}{L_f^{2H}}\rightarrow\begin{matrix}\Delta x=k\Delta x_o\\ L_f=k_c\Delta x_o=\sqrt{k_s}\sigma_z/c\end{matrix}$$

where for stationary functions $k_s=2$ [5].

Removing the average trend from the profiles we have planned to obtain the mean value of the RMS height from Mola data

(2.2-19)
$$\sigma_z=\sqrt{\frac{1}{N}\sum_{i=1}^{N}(z(i))^2}$$

The Hurst coefficient can be estimated trough the Allan variance (Gallant) (semivariogram) that can be computed trough the N profile samples according to ($\Delta x = k\cdot\Delta x_o \rightarrow k$)

(2.2-20)
$$v(k)=\sqrt{\langle[z(x)-z(x+\Delta x)]^2\rangle}=v(\Delta x_0)\left(\frac{\Delta x}{\Delta x_0}\right)^H\equiv v(1)\cdot k^H\rightarrow$$

$$v^2(k) = \frac{\sum_{i=1}^{N-k} (z(i) - z(i+k))^2}{N-k}$$

so that

(2.2-21) $$\log v(k) = H \cdot \log k + \log v(1) \Leftrightarrow v(k) = v(k\Delta x_0) \Leftrightarrow s(\Delta x) = \frac{v(\Delta x)}{\Delta x}$$

being the slope

$$s(\Delta x) = v(\Delta x_0) \frac{\Delta x^{H-1}}{\Delta x_0^{H}} = s(\Delta x_0) \left(\frac{\Delta x}{\Delta x_0} \right)^{H-1} \rightarrow$$

$$s(\lambda) = \sqrt{2}\, \sigma_z \frac{(\lambda)^{H-1}}{L_f^{H}}$$

Thence trough a linear best fitting, performed in a proper lag distance, of the logarithm of the Allan variance, H and υ(1) (and the slope) values for each subsection can be estimated.

Moreover the same profiles and the same sections can be processed to obtain the correlation function according to:

(2.2-22) $$\rho(k) = \frac{\sum_{i=1}^{N-k} (z(i) \cdot z(i+k))}{\frac{1}{2}\sum_{i=1}^{N-k} (z(i))^2 + \frac{1}{2}\sum_{i=1+k}^{N} (z(i))^2}$$

To model the correlation function with the analytical model (s.(2.2-18)) we can write:

(2.2-23)

$$\log(\ln \frac{1}{\rho(k)}) = 2H \log k - 2H \log k_c$$

Again from a linear best fitting in a logarithm scale estimation of the parameters H and k_c can be obtained.

In order to validate the selected algorithms we have selected a surface region (3.5-4 S, 112.5-113 E) of 10*10 Km (due to the preliminary information of the correlation length and MARSIS spatial resolution). Taking into account of the behaviour of fig.3a), by best fitting we have obtained the flat surface of fig.3b), so that on the difference (s. fig.3c)) we have applied the previous estimation technique (for each selected profile in column and line direction, performing proper mean values) obtaining the fractal estimated parameters shown always in fig.3. We have obtained H values near 1, so that the geometric optical model can be applied.

The previous approach was applied to Guesv crater (13-16 S, 173-177 E, characterized by big slope around the crater) of 170*250 Km^2, in all (overlapped in column and line direction of 5 km) sub regions of 10*10 Km^2 , obtaining the results of fig.4.

We are arrived to the conclusion that the well known backscattering models under Kirchhoff formulation can be applied [3][4].

Moreover we wish recall the following range of surface size involved in MARSIS Altimeter by considering pulsed limited region and cross track region over imposed to subsurface region to be investigated:

Radar range resolution = r

$$R_{PL} = \sqrt{2rR_p} \rightarrow R_p = \frac{h \cdot R_{MARS}}{h + R_{MARS}} \approx h \rightarrow R_{PL} = 8-15km$$

Pulsed Limited radius

$$R_\delta = \sqrt{2\delta R_p} \quad \delta = ir \rightarrow \text{ depth } \rightarrow \delta = 5km \rightarrow R_\delta = 44-90km$$

Cross-track range, from nadir pointing, displacement of the surface clutter region referred to subsurface depth δ*: the permittivity constant of the first layer will be taken into account in* δ*.*

$$\theta_\delta = \frac{\sqrt{2\delta R_p}}{h} \approx \sqrt{\frac{2\delta}{h}} = \sqrt{\frac{2r}{h}} \cdot \sqrt{i} \rightarrow \theta_\delta = 0.05-0.45 rad$$

Cross-track angle

$$\beta_\delta = \sqrt{\frac{2r}{h}} \cdot \left(\sqrt{i+1} - \sqrt{i} \right) \approx \sqrt{\frac{r}{2h \cdot i}} = \frac{r}{\sqrt{2h \cdot \delta}} = \frac{r}{R_\delta}$$

$$\beta_\delta = 1.5 - 4 \cdot 10^{-3} rad$$

$$L_{Cl} \approx \beta_\delta \cdot H \approx r\sqrt{\frac{H}{2\delta}} \qquad L_{Cl} \approx 0.7 - 1.4 km$$

Cross-track size

where the cross-track angle and size are referred to the circular rings.

Concerning the backscattering from the surface, pulse limited region, (taking into account that we are in side or outside Fresnel region and the small observation angle referred to nadir pointing) we wish recall the cross-section [3][11],(related to the maximum value of eq.(2.2-15)):

- <u>nadir observation</u>

(2.2-24)

$$\sigma_{PL}\big|_{\max} = \Gamma(0) \left[\frac{e^{-4k^2\sigma_h^2}}{\sqrt{\frac{\lambda^2}{4\pi \cdot L_\theta^2} + \frac{L_\theta^2}{\pi h^2}} \sqrt{\frac{\lambda^2}{4\pi \cdot L_{\theta_c}^2} + \frac{L_{\theta_c}^2}{\pi h^2}}} + \frac{\left(1 - e^{-4k^2\sigma_h^2}\right)}{\sqrt{\frac{\lambda^2}{4\pi \cdot L_\theta^2} + \frac{L_\theta^2}{\pi h^2} + 2m_s^2} \sqrt{\frac{\lambda^2}{4\pi \cdot L_{\theta_c}^2} + \frac{L_{\theta_c}^2}{\pi h^2} + 2m_s^2}} \right]$$

where L_θ ($L_{\theta c}$) is the backscattering region size defined in along (cross-) track observation direction.

- <u>cross track observation,</u> in the region related to subsurface investigation (depth δ),:

(2.2-25)

$$\sigma_{C\delta} = \Gamma(0) \left[\frac{e^{-4k^2\sigma_h^2} \cdot e^{-\frac{\left(\sqrt{\frac{2\delta}{h}} - \alpha_{C\delta}\right)^2}{\frac{1}{2\pi h}\frac{\lambda^2\delta}{r^2}}}}{\sqrt{\frac{1}{2\pi h}\frac{\lambda^2\delta}{r^2}} \sqrt{\frac{\lambda^2}{4\pi \cdot L_{\theta_c}^2} + \frac{L_{\theta_c}^2}{\pi h^2}}} + \frac{\left(1 - e^{-4k^2\sigma_h^2}\right) \cdot e^{-\frac{\left(\sqrt{\frac{2\delta}{h}} - \alpha_{C\delta}\right)^2}{\frac{1}{2\pi h}\frac{\lambda^2\delta}{r^2} + 2m_s^2}}}{\sqrt{\frac{1}{2\pi h}\frac{\lambda^2\delta}{r^2} + 2m_s^2} \sqrt{\frac{\lambda^2}{4\pi \cdot L_{\theta_c}^2} + \frac{L_{\theta_c}^2}{\pi h^2} + 2m_s^2}} \right]$$

as worst case we can assume the maximum value of the $\alpha_{Cl\delta}$ in the region under investigation, in order to evaluate the maximum level of the clutter involving the corresponding subsurface region.

Moreover where the H ≠1, taking into account that, by considering small angle referred to nadir observation, we can use always the previous eq. where the slope m_s becomes:

(2.2-26) $$m_f = \left(2\sqrt{2}\pi\right)^{(1/H)-1} (s(\lambda))^{1/H} \sqrt{\frac{H}{\Gamma\left(\frac{1}{H}\right)}}$$

where s(λ) is the value of the rms slope evaluated between points separated by a distance equal to the transmitted wavelength:

(2.2-27) $$s(\lambda) = \sqrt{2}\, \sigma_{hi} \frac{(\lambda)^{H-1}}{L_i^H}$$

Moreover we can notice different statistical properties in x and y direction in some regions of Guesv crater, e.g. crater edge as shown in fig.4, where the subsurface investigation is not easy, due to the particular slope in x direction. In this case, in order to estimate the backscattering, facets methods should be applied.

3 CONCLUSIONS

In order to evaluate the surface backscattering, the following procedure (by MOLA data) can be applied:

- Selection of the 10*10 km^2 regions, overlapped of 5 Km in the perpendicular directions
- Flat surface estimation for each region by best fitting
- With reference to the flat surface for each region must be estimated:
  - z_i mean value of the surface height
  - α_{xi}, α_{yi} surface slopes in x and y direction
- With reference to the difference between input MOLA data and the flat surface for each region must be estimated:
  - σ_i rms surface
  - L_i correlation length
  - H_i Hurst coefficient

The previous estimation will be obtained in the orbit motion direction (mean value of multi profiles selected by considering the radar spatial resolution) or the same procedure will be applied a priori in two selected perpendicular direction and finally a proper or the mean value of the previous results will be available.
If the estimated correlation length is bigger of the size of selected region (10 km), facets development (accuracy best of $\lambda/4$) should be applied.

REFERENCES

[1] Ulaby F.T., Moore R.K., and Fung A.K., Microwave remote sensing: active and passive, Vol.II-III, Addison Wesley Publishing Co., London,1986

[2] Fung A.K., Li Z., Chen K.S., Backscattering from a randomly rough dielectric surface, IEEE GE v.30 n.2, March '92

[3] Fung, A.K., Eom, H.J., Coherent Scattering of a spherical wave from an irregular surface, IEEE AP v.31, Jan '83

[4] Ciaffone A., Picardi G., Seu R., Application of the PARIS concept to the GPS signals, STS Rome Italy, Technical Report #TR-1-3/1/95, ESAcontract 142286-27/06/94

[5] Shepard M.K. et alii – Self-affine (fractal) topography - Journal of Geophysical Research June 25, 1995

[6] Shepard M., Campbell B. Radar Scattering from a Self-affine Fractal Surface…Icarus 141 - 1999

[7] Plaut J., S.Garneau S., -MOLA-derived roughness data used to predict surface scattering for Mars subsurface radar sounding, in The Fifth International Conference on Mars (CD-ROM), abstract #6239, Lunar and Planetary Institute, Houston, 1999.

[8] Biccari D., Picardi G., Seu R., Melacci P.T., 2001a. Mars surface models and subsurface detection performance in MARSIS. Proceedings of IEEE International Symposium on Geoscience and Remote Sensing, IGARSS 2001, Sydney, Australia, 9-13 July 2001.

[9] Picardi G., Sorge S., Seu R., Fedele G., Federico C., Orosei R., 1999a. Mars Advanced Radar for Subsurface and Ionosphere Sounding (MARSIS): Models and system analysis. Infocom Technical Report N.007/005/99

[10] Campbell B., Ghent R., Shepard M.K., Limits on inference of Mars small-scale topography from MOLA data, Geophysical Research Letters (in press).

[11] Montefredini E., Picardi G., Seu R. Evaluation of approximation errors of coherent and non-cohereht scattering models under Kirchoff formulation ISNCR '94

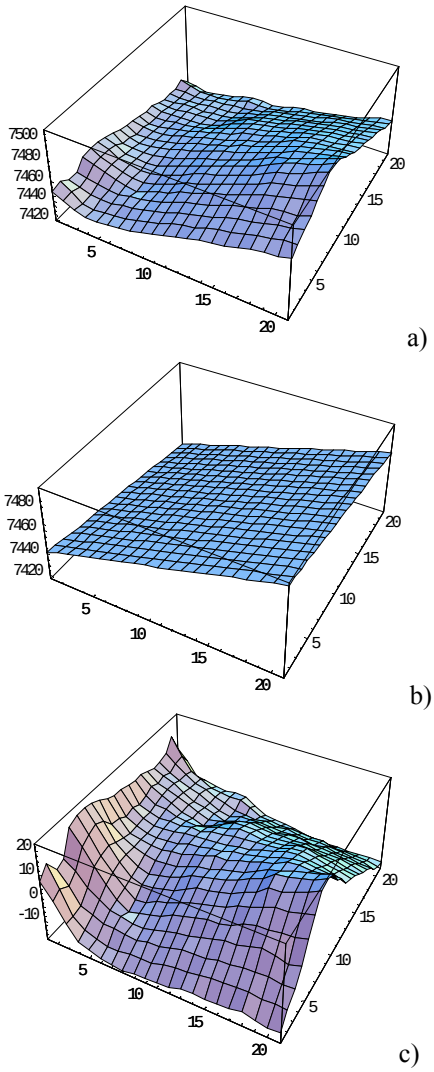

Direction	σ (m)	H	L_f (m)	k_s	m
X	5.27	0.78	1851	1.88	0.004
Y	7.05	0.86	1716	1.77	0.006
Average	6.16	0.82	1783	1.82	0.005

Fig.3 (3.5-4 S,112.5-113 E)

GUSEV CRATER

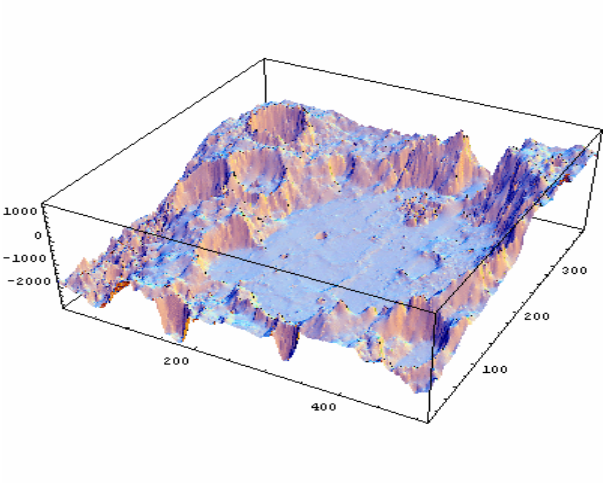

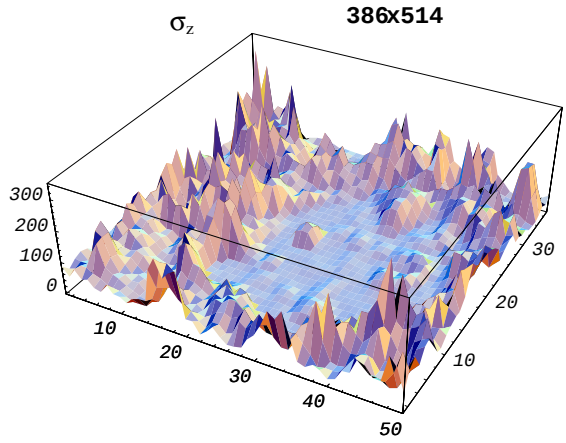

H

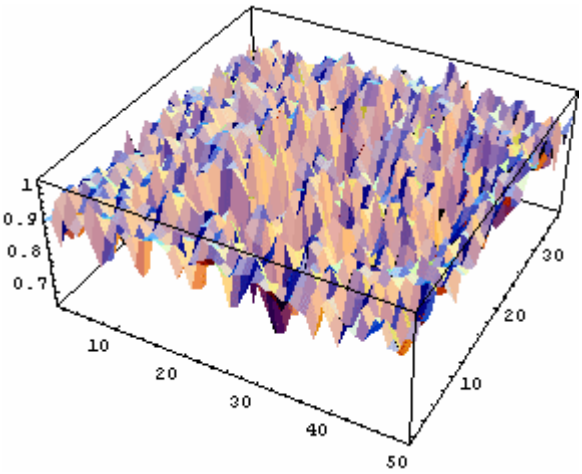

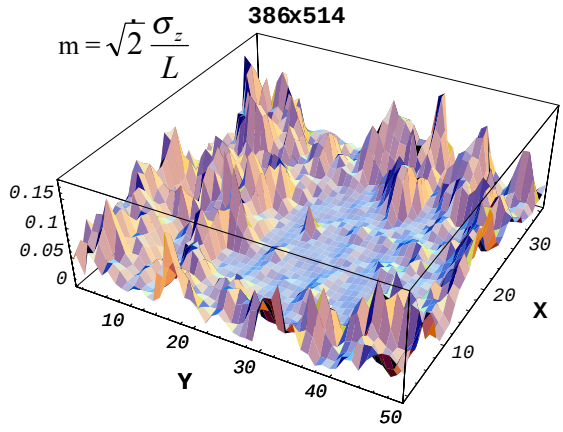

$\alpha_i = \sqrt{\theta_i^2 + \varphi_i^2}$ (degree)

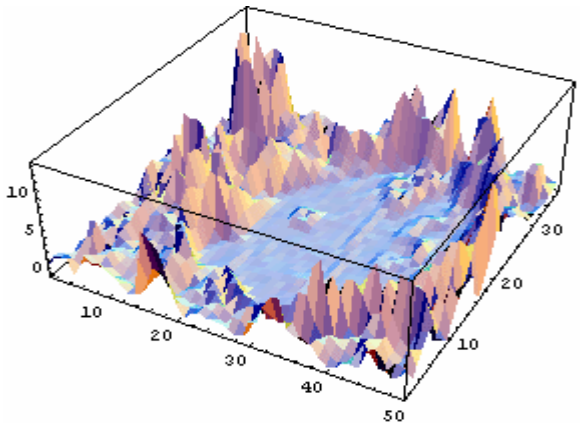

Direction	σ (m)	H	L (m)	M
X (α_x=-0.13 rad)	115	0.99	1384	0.004
Y (α_y=0.02 rad)	70	0.79	106845	-

Fig. 4 (13-16 S, 173-177 E)